

# Anti-tumor activity of self-charged (Eu,Ca):WO<sub>3</sub> and Eu:CaWO<sub>4</sub> nanoparticles

CAO LIN\*, CAO JIEXIN<sup>†</sup>, WANG CONG, CHE PING<sup>‡</sup>, PAN DE'AN and ALEX A VOLINSKY<sup>#</sup>

Department of Materials Physics, University of Science and Technology Beijing, Beijing 100083, China

<sup>†</sup>Peking University Health Science Centre, Beijing 100191, China

<sup>‡</sup>School of Applied Science, University of Science and Technology Beijing, Beijing 100083, China

<sup>#</sup>Department of Mechanical Engineering, University of South Florida, Tampa FL 33620, USA

MS received 26 May 2011; revised 25 July 2011

**Abstract.** Non-stoichiometric (Eu,Ca):WO<sub>3</sub> and Eu:CaWO<sub>4</sub> nanoparticles with anti-tumor activity are synthesized in a sol-gel method by adding excessive Eu<sup>3+</sup> and Ca<sup>2+</sup> ions to tungsten oxide crystal structure. Colorimetric assay shows that 10 nm (Eu,Ca):WO<sub>3</sub> and Eu:CaWO<sub>4</sub> nanoparticles can effectively inhibit growth of mammary cancer cells without any harm to normal cells. Nanoparticles are characterized by X-ray diffraction, high resolution transmission electron microscopy and fluorescence optical spectrometry. Nanomaterials, insoluble in synthesized water, have complicated self-charging surfaces that trap mammary cancer cells. Surface self-charging effect is suggested as the inhibition mechanism.

**Keywords.** Anti-tumor activity; self-charged; nanoparticles.

## 1. Introduction

In the 1970s, French scientists discovered anti-tumor and anti-viral characteristics of polyacid compounds (Raynaud *et al* 1971; Chermann *et al* 1975; Schoenfeld *et al* 1975). In the late 1980s, Yamase suggested a circular redox mechanism from a perspective of biomolecule electronic structure based on certain anti-tumor experiments (Yamase *et al* 1988; Inouye *et al* 1991). However, there is no appropriate technique to prove this theory. In recent years, studies of anti-tumor drugs mainly focused on nanomaterials. Several nanomaterials with anti-tumor effects have been synthesized. For example, Yin *et al* (2006) and Ingo *et al* (2006) reported that hydroxyapatite nanoparticles can inhibit hepatocellular carcinoma cells. Cao *et al* (2007) prepared Eu<sup>3+</sup> doped nano-scheelite which can effectively inhibit human promyelocytic leukemia cell line (HL60). In this paper, the inhibiting effects of (Eu,Ca):WO<sub>3</sub> and Eu:CaWO<sub>4</sub> nanoparticles on HL60 are reported and the anti-tumor mechanism is discussed based on the self-charging surface concept.

## 2. Results

### 2.1 Crystal structure and phase analysis

Figure 1 shows XRD diffraction pattern of the as-synthesized (Eu,Ca):WO<sub>3</sub> and Eu:CaWO<sub>4</sub> nanoparticles. The main diffraction reflection corresponds to the (Eu,Ca):WO<sub>3</sub> phase.

The diffraction reflection of the Eu:CaWO<sub>4</sub> phase is quite weak, which means that most of the nanoparticles are formed in the (Eu,Ca):WO<sub>3</sub> phase, and only a small portion of them is the Eu:CaWO<sub>4</sub> phase. The main diffraction reflection can be well indexed to the monoclinic WO<sub>3</sub> phase: space group  $P2(1)/n$ ,  $a = 7.297 \text{ \AA}$ ,  $b = 7.539 \text{ \AA}$ ,  $c = 7.68809 \text{ \AA}$ ,  $\alpha = 90^\circ$ ,  $\beta = 90.91^\circ$ ,  $\gamma = 90^\circ$  (PDF number 83-0951). No diffraction reflections corresponding to Eu or Ca-related phases are detected, indicating that the Eu and Ca ions have been doped into the crystal lattice without changing the WO<sub>3</sub> structure.

Crystal structure of (Eu,Ca):WO<sub>3</sub> is similar to ReO<sub>3</sub>, which belongs to the cubic crystal system with positive and negative ion coordination numbers of 6 and 2, respectively. In this structure, the [ReO<sub>6</sub>] octahedrons are interconnected with each other by Re culmination in three dimensions. This structure has large inter-atomic spaces in the centre of the unit cell, i.e. the structure channels. WO<sub>3</sub> structure can be obtained by a small distortion of the ReO<sub>3</sub> structure. Eu and Ca ions in the inter-atomic spaces of WO<sub>3</sub> can form (Eu,Ca):WO<sub>3</sub> as is shown in figure 2. TEM shows that (Eu,Ca):WO<sub>3</sub> and Eu:CaWO<sub>4</sub> phases can be jointly positioned in each nanoparticle or be respectively positioned in different nanoparticles.

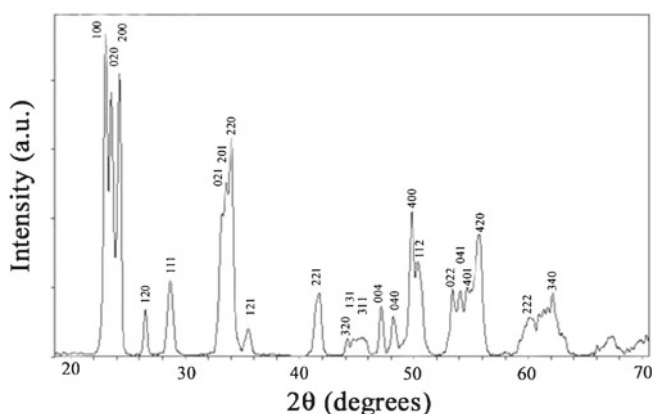
### 2.2 (Eu,Ca):WO<sub>3</sub> nano-crystal morphology and formation mechanism

Figure 3 shows synthesized (Eu, Ca):WO<sub>3</sub> morphologies at different synthesis stages. In the process of preparing the

\*Author for correspondence (lincaoustb@yahoo.com.cn)

sample, as the  $\text{Ca}^{2+}$  ions are gradually added to the precursor,  $\text{Eu}^{3+}$ ,  $\text{Ca}^{2+}$ , acetic acid and ammonium paratungstate are formed.  $(\text{Eu}^{3+}, \text{Ca}^{2+})\text{:WO}_3$  system with superabundant positive charge is formed after  $\text{Eu}^{3+}$  or  $\text{Ca}^{2+}$  occupied the inter-atomic spaces of  $\text{WO}_3$  decomposed by the ammonium paratungstate. The new decomposed  $\text{WO}_3$  in the solution has been adsorbed on the surface of the  $(\text{Eu}^{3+}, \text{Ca}^{2+})\text{:WO}_3$  system for attracting the positive charge. Thus the micelle system is positively charged and turns into a positive micelle. This is an ‘adsorption sol’ process. CTAB polarity end in the solution is negatively charged and forms an adsorption layer which is adsorbed on the sol surface. The carbon–hydrogen group at the colloid surface of the adsorption layer can reduce surface energy of nanoparticles, weaken the electrostatic effect and avoid enlargement and conglomeration of the nanoparticles. At first when calcium acetate drops into the solution, the relative concentration of CTAB is higher

than 1.66%. According to the Debye’s sausage shape model (Debye and Anacker 1951), one may assume that this solution system has a structure of CTAB micelle double layer shown in figure 3A. It is shaped like a disc in the centre with radiating molecules, while at the two poles it takes the form of a Hartley sphere (Hartley 1936). There is a large quantity of surfactant molecule polarity groups in this model so that a better contact with the colloid is achieved. At the same time the contact area of the carbon–hydrogen chain with water is reduced. It is more thermodynamically stable, thus a stick-shaped Eu, Ca-doped nano-tungsten oxide with a diameter of  $\sim 10$  nm is synthesized, as shown in figure 3B. At the anaphase of the reaction the relative concentration of CTAB is about 0.83% and the stick-shaped nanomaterials change into spherical micelles. Consequently, spheres of Eu, Ca-doped nano-tungsten oxide with a diameter of  $\sim 10$  nm are formed.



**Figure 1.** XRD diffraction pattern of  $(\text{Eu,Ca})\text{:WO}_3$  and  $\text{Eu:CaWO}_4$  nanoparticles.

### 2.3 Microstructure and electronic structure of $(\text{Eu}, \text{Ca})\text{:WO}_3$ phase

Based on the structure analysis, Ca and Eu atoms cannot substitute W atoms on the triad axis of the  $\text{WO}_3$ , they can only occupy centre of the structure channel inter-atomic spaces formed by  $\text{WO}_3$  rhombic system.

Figure 4 is the high-resolution TEM image of a  $(\text{Eu,Ca})\text{:WO}_3$  nanoparticle taken along the  $[\bar{1}21]$  direction; figure 5 is the simulated image of the  $[\bar{1}21]$  projection. The black pairs of pellets are the W atoms; the grey ones are the O atoms. Two W atoms share six O atoms and together form an octahedron structure. Every four of these octahedrons can form a big square structure channel. Figure 6 is the high resolution TEM image of a  $(\text{Eu,Ca})\text{:WO}_3$  nanoparticle taken along the  $[31\bar{2}]$  direction, showing that the open square channel in the crystal structure is occupied by Eu and Ca. As

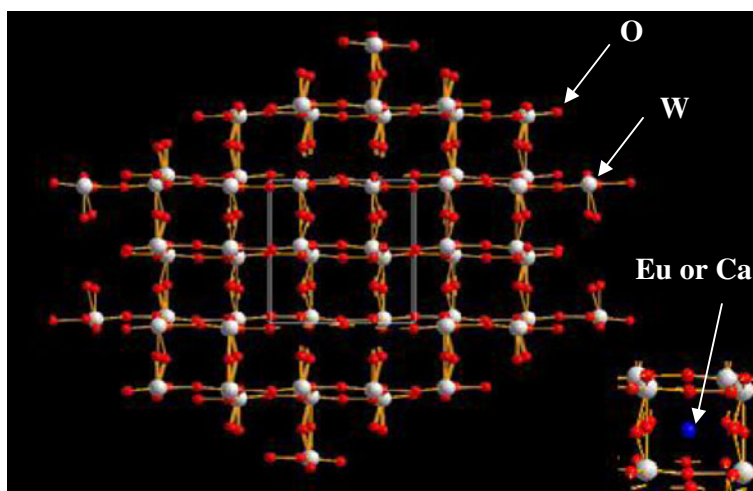


**Figure 2.** Simulated  $(\text{Eu,Ca})\text{:WO}_3$  structure image, where biggest white balls are W atoms, smaller red balls are O atoms and centre blue balls are Eu or Ca atoms.

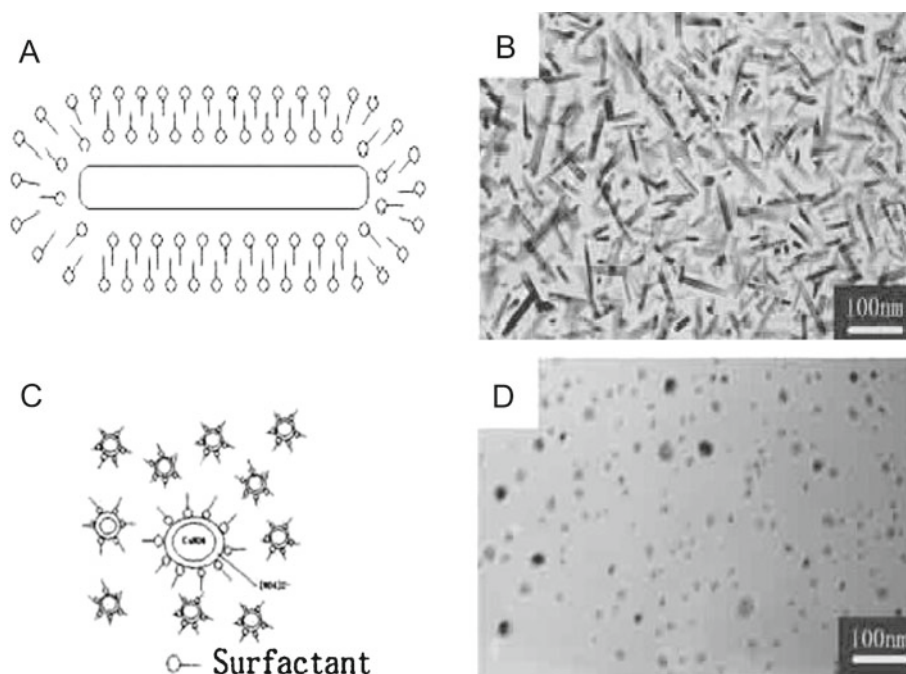


**Figure 3.** (A, B). First stage as calcium acetate drops in (CTAB relative concentration is relatively high); (C, D) later stages as calcium acetate drops in (CTAB relative concentration is relatively low).

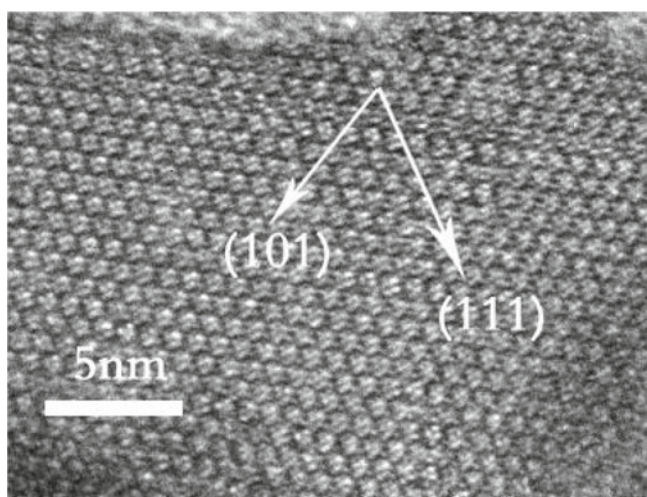


**Figure 4.** High resolution TEM image of a (Eu,Ca):WO<sub>3</sub> nanoparticle taken along  $[\bar{1}21]$  direction.

there are so many Ca<sup>2+</sup> and Eu<sup>3+</sup> ions that the crystal surface has, excessive charges cannot easily be compensated. Thus, this part of the crystal loses its symmetry centre due to small lattice distortions caused by charge imbalance.

Because preparation of the sample is an adsorption sol process, nanograins will form different channels after being heated. Figure 7 is the grain boundary channel formed by three crystal boundaries converged inside the particle.

These channels can form nano-traps with an adsorbing effect.

#### 2.4 Role and charge clustering of Eu<sup>3+</sup>, Ca<sup>2+</sup> ions in Eu:CaWO<sub>4</sub>

Although (Eu,Ca):WO<sub>3</sub> is a non-illuminant, a spectrograph can be used to measure the spectrum of Eu:CaWO<sub>4</sub>. Figure 8 gives 394 nm excited emission spectra of bulk Eu:CaWO<sub>4</sub> and Eu:CaWO<sub>4</sub> nanoparticles.

It can be concluded from table 1 and figure 8 that the spectral peak of both bulk and nanomaterials for the  $^5D_0 \rightarrow ^7F_2$  transition splits into three peaks. The selection rules state that in such a case the point group of the nanomaterial structure is  $D_2$ , the luminescence centre is a rhombic system with no symmetric or inversion centre (Zhang 1983). There is little difference between the radii of Eu<sup>3+</sup> and Ca<sup>2+</sup> ions (96 pm for Eu<sup>3+</sup> and 99 pm for Ca<sup>2+</sup>), and their charge only differs by 1, therefore, Eu<sup>3+</sup> ions can easily occupy the lattice sites of Ca<sup>2+</sup> ions. This causes aberration in the Ca<sup>2+</sup> ion-induced hexahedron, magnifying the (010) lattice plane and makes it lose its inversion centre. Thus a charge clustering is created and the original CaO<sub>8</sub> regular hexahedron turns into a hexahedron without a symmetric centre. As the  $^5D_0 \rightarrow ^7F_2$  transition is stronger in the nanomaterial than in the bulk, it can be inferred that this sort of aberration is more evident in the former than in the latter. Figure 9A shows acyclic variations of the spacing and contrast of the (101) lattice planes brought by local charge surplus as a result of

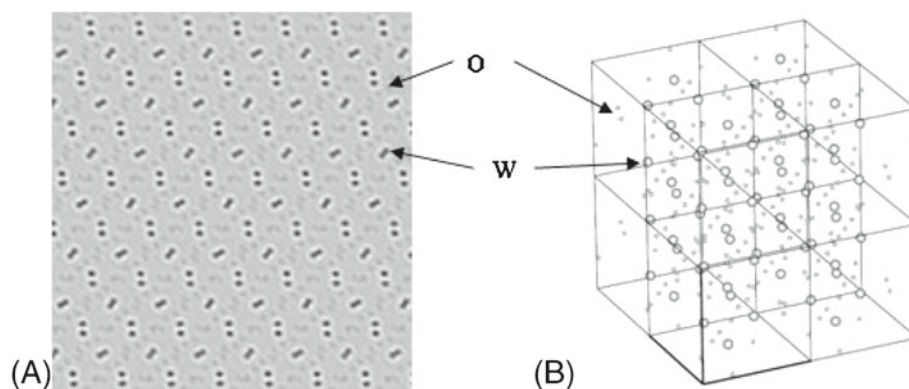


**Figure 5.** (A) Simulated  $[\bar{1}21]$  projected image and (B) 3D schematic of  $\text{WO}_3$  crystal structure.

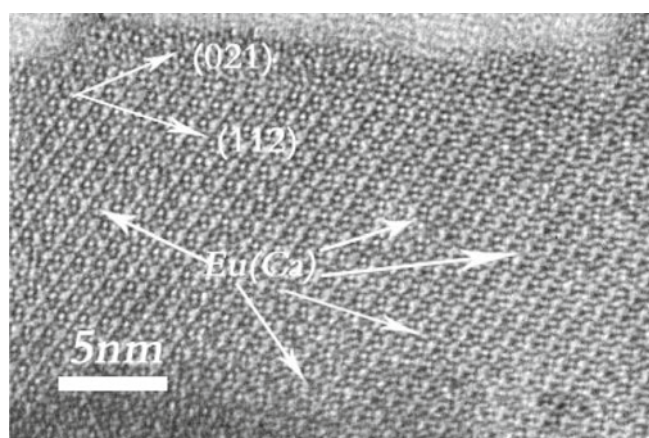


**Figure 6.** High resolution TEM image of a  $(\text{Eu,Ca})\text{:WO}_3$  nanoparticle taken along  $[31\bar{2}]$  direction.

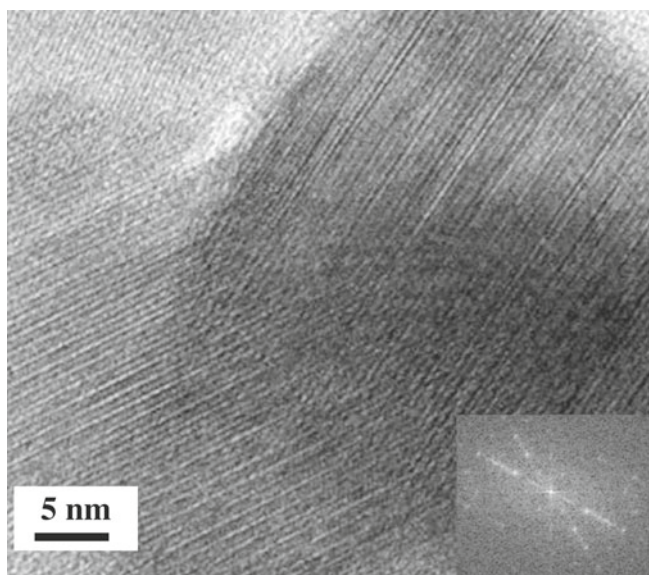


**Figure 7.** Grain boundary channel formed by three crystal boundaries convergence in  $\text{WO}_3$  crystal.

$\text{Ca}^{2+}$  ions surplus, causing clustering along the 101 direction and substitution of  $\text{Ca}^{2+}$  by  $\text{Eu}^{3+}$ . Figure 9B shows  $\text{Ca}^{2+}$  substitution by  $\text{Eu}^{3+}$ , and a short dislocation of the (101) lattice direction caused by  $\text{CaO}_8$  aberration generated by surplus  $\text{Ca}^{2+}$  ions.

### 3. Anti-tumor experimental results

The results of this study indicates that there is no relationship between drug dose and its effects on human umbilical veins endothelial cell, one kind of normal human cells, as shown in figure 10. This experiment indicates that the drug causes no harm to normal cells.

However, as the concentration of the drug is increased, inhibiting effect on mammary cancer cells is enhanced gradually, presenting a dose response relationship.

This experiment indicates that the drug can inhibit mammary cancer cells and that the inhibiting ratio is enhanced gradually with increasing drug concentration.

#### 3.1 Surface self-charging theory of anti-tumor activity

According to the above analysis, we can propose the surface self-charging theory of  $(\text{Eu,Ca})\text{:WO}_3$  and  $\text{Eu:CaWO}_4$  nanoparticles. Tumor cells have abnormal electronic structure with non-localized, highly active electrons. Lanthanide,  $\text{Ln}^{3+}$  ions, originating from biological macromolecules (proteins, enzymes and nucleic acids, etc.) can replace metal ions such as  $\text{Ca}^{2+}$  and  $\text{Mg}^{2+}$ . These ions can be combined with groups such as amino acid, phosphoric acid, etc in biological macromolecules, thus forming biological macromolecule groups. Because of these special features, when the structure traps of the nano-grains adsorb a tumor cell by electrostatic forces, the tumor protein comes into contact with  $\text{Ln}^{3+}$  ions. Reactions on the self-charged surface of nanoparticles can inhibit duplication of tumor cells through electrons transfer.

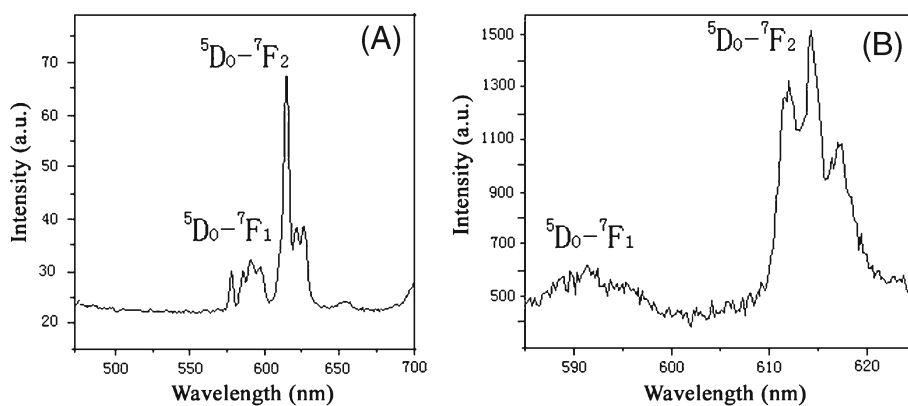


**Figure 8.** 394 nm excited emission spectra of (A) bulk Eu:CaWO<sub>4</sub> and (B) Eu:CaWO<sub>4</sub> nanoparticles.

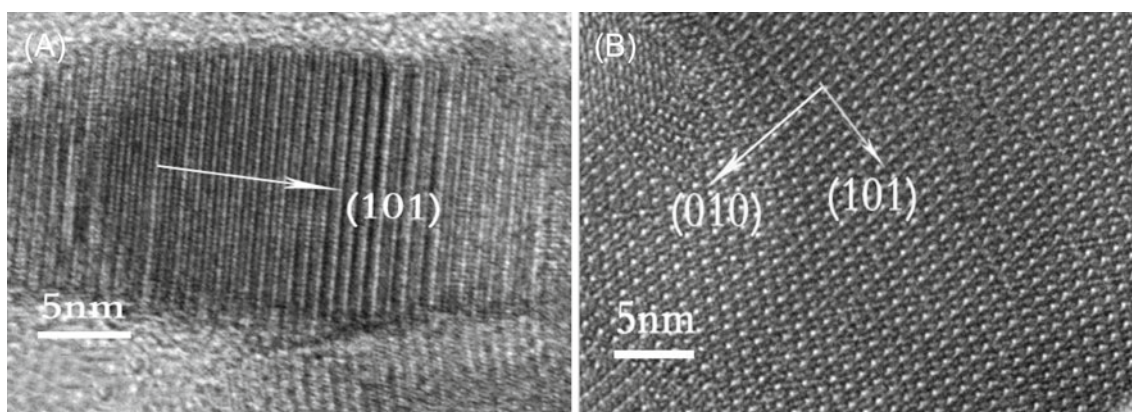


**Figure 9.** (A) Bright field high resolution TEM image of Eu:CaWO<sub>4</sub> obtained with electron beam parallel to (101) lattice direction and not parallel to other lattice directions and (B) bright field high resolution TEM image of Eu:CaWO<sub>4</sub> obtained with electron beam parallel to both (101) and (010) lattice directions.

**Table 1.** Possible Eu<sup>3+</sup> ion symmetry positions and their transition characteristics.

Crystal system	Symmetric group	Magnetic dipole transition $J = 0 \rightarrow J = 1$	Electronic dipole transition $J = 0 \rightarrow J = 1$	Electronic dipole transition $J = 0 \rightarrow J = 2$
Monoclinic	$C_2$	$3 (\pi 1, \sigma 2)$	$3 (\pi 1, \sigma 2)$	$5 (\pi 3, \sigma 2)$
	$C_s(C_{1h})$		$3 (\pi 2, \sigma 1)$	$5 (\pi 2, \sigma 3)$
	$C_{2h}$		Forbidden	Forbidden
Orthorhombic	$D_2$	$3 (\pi 1, \sigma 2)$	$3 (\pi 1, \sigma 2)$	$3 (\pi 1, \sigma 2)$
	$C_{2v}$		$2 (\sigma 2)$	$4 (\pi 2, \sigma 2)$
	$D_{2h}$		Forbidden	Forbidden

#### 4. Discussion

Cancer is one of the most fatal diseases of the present day. Although several chemotherapy or subsidiary anti-cancer drugs are used clinically, most of them can only provide a temporary relief instead of permanent cure. Nobel laureate in Physiology or Medicine, Szent-Györgyi believes that many factors can cause cancer, but just like there are several reasons for a moving car to stop, the most essential one

is braking, and the 'brake' which stops cancer is most likely the electron transfer effect. (Eu,Ca):WO<sub>3</sub> and Eu:CaWO<sub>4</sub> nanoparticles are different from other drugs in that they have a structure which can exchange electrons with tumor cells. This new discovery may establish a novel direction for anti-tumor drug research and bring a far-reaching effect in search for the cure of tumors.

The main prospect of this study is that current formulation for cancer treatment can be improved. At the same

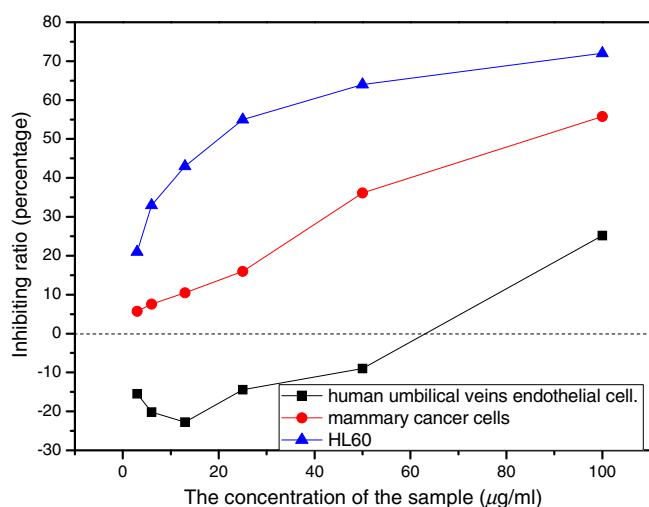


**Figure 10.** Drug concentration effect on inhibition of mammary cancer/human umbilical endothelial cells and HL60.

time Eu:CaWO<sub>4</sub> nanoparticles are also fluorescent, which can provide a new method for *in vivo* tumor research. For instance, we can utilize this material as a spectrum probe for biological dim light stationary processes using a single photon detector. We can also use the *ns-ps-fs* transient absorption line to study the ultra-fast processes that occur in biological systems. Resonance energy spectrometry could be employed to study the electron transfer rules of (Eu,Ca):WO<sub>3</sub> and Eu:CaWO<sub>4</sub> nanoparticles and their anti-tumor characteristics. This research pioneers a new path of medication study, and may have a great impact on anti-tumor research.

#### 4.1 Methods

1 g of ammonium paratungstate was dissolved in 5 ml of glycol in a round bottom flask followed by 0.1 g of cetyltrimethyl ammonium bromide (CTAB). Calcium acetate (0.5 g) was dissolved in another 5 ml glycol solution with 5 ml 0.1 mol/L EuCl<sub>3</sub> in a glass container. The solution from this glass container was then added drop by drop into the round bottom flask under continuous magnetic stirring for 10 min at 60 °C. Mixed solution was then placed in a 100 ml capacity Teflon-lined stainless steel autoclave at a temperature of 110 °C for 4 h, and then cooled at room temperature for 12 h. The sediment was obtained by filtering the product, which was heat-treated at 110 °C for 4 h in a dry oven and then heat-treated again in an electric oven at 550 °C for 4 h.

The product was ground for 30 min to acquire nano-sized (Eu,Ca):WO<sub>3</sub> and Eu:CaWO<sub>4</sub> powders. The anti-tumor drug was obtained by putting the products into dimethyl sulfoxide (DMSO) to form a colloidal solution.

X-ray diffraction (XRD) pattern was obtained using an X-ray diffractometer (D/max, Rigaku, Japan). TEM images were taken on a JEM-100 transmission electron microscope (JEOL Ltd, Tokyo, Japan). High resolution images were taken on JEM-2010 high resolution transmission electron microscope (JEOL Ltd, Tokyo, Japan). The sample emission and excited spectra were obtained with Fluorolog-3 fluorescence optical spectrometer at room temperature.

Anti-tumor experiments were carried out at the Peking University Health Science Centre. The effect of the drug on cell proliferation was determined by using MTT (3-(4,5-dimethylthiazol-2-yl)-2,5-diphenyltetrazolium bromide) colorimetric assay. Exponentially growing cells were seeded onto a 96-well microplate at 10<sup>5</sup> cells/well. After 6 h, cells were exposed to increasing concentrations of compounds for 48 h. Then 20 µl of 5 mg/ml MTT in pure bovine serum was added. After an additional 4 h of incubation, reaction was quenched with an assay buffer (5% isopropanol, 0.1% hydrochloric acid and 10% sodium dodecyl sulfate) overnight, and the absorbance was measured at 570 nm wavelength by using a microplate multi-detection reader and compared with 630 nm wavelength absorbance.

#### References

- Cao L et al 2007 *Int. J. Miner. Metall. Mater.* **16** 468
- Chermann J C, Shinoussi F N and Jasmin C 1975 *Biochem. Biophys. Res. Commun.* **65** 1229
- Debye P and Anacker E W 1951 *J. Phys. Colloid. Chem.* **55** 644
- Hartley G S 1936 *Aqueous solutions of paraffin chain salts* (Paris: Hermann)
- Ingo W B, Yingchao H and Shipu L 2006 *J. US-China Medical Sci.* **3** 42
- Inouye Y, Tokutake Y, Yoshida T, Yamamoto A, Yamase T and Nakamura S 1991 *Chem. Pharm. Bull.* **39** 1638
- Raynaud M et al 1971 *C. R. Acad. Sci. Ser. D* **272** 347
- Schoenfeld B, Steinheider G and Glemser O Z 1975 *Naturforsch.* **306** 959
- Yamase T, Fujita H and Fukushima K 1988 *Inorg. Chim. Acta* **151** 15
- Yin M Z, Han Y C, Bauer I W, Chen P and Li S P 2006 *Biomed. Mater.* **1** 38
- Zhang Siyuan 1983 *Lumin. Display Dev. (in Chinese)* **3** 18